The Journal of Experimental Biology 211, 3661-3670
Published by The Company of Biologists 2008
doi:10.1242/jeb.018754

The mechanics of the gibbon foot and its potential for elastic energy storage during bipedalism

Evie E. Vereecke[1,2,*] and Peter Aerts[2,3]

[1]Department of Human Anatomy and Cell Biology, School of Biomedical Sciences, University of Liverpool, Liverpool L69 3GE, UK,
[2]Laboratorium for Functional Morphology, University of Antwerp, Universiteitsplein 1, B-2610 Antwerp, Belgium and
[3]Department of Movement and Sports Sciences, University of Ghent, Watersportlaan 2, B-9000 Gent, Belgium

*Author for correspondence (e-mail: evie.vereecke@liv.ac.uk)

Accepted 30 September 2008

SUMMARY

The mechanics of the modern human foot and its specialization for habitual bipedalism are well understood. The windlass mechanism gives it the required stability for propulsion generation, and flattening of the arch and stretching of the plantar aponeurosis leads to energy saving. What is less well understood is how an essentially flat and mobile foot, as found in protohominins and extant apes, functions during bipedalism. This study evaluates the hypothesis that an energy-saving mechanism, by stretch and recoil of plantar connective tissues, is present in the mobile gibbon foot and provides a two-dimensional analysis of the internal joint mechanics of the foot during spontaneous bipedalism of gibbons using a four-link segment foot model. Available force and pressure data are combined with detailed foot kinematics, recorded with a high-speed camera at 250 Hz, to calculate the external joint moments at the metatarsophalangeal (MP), tarsometatarsal (TM) and talocrural (TC) joints. In addition, instantaneous joint powers are estimated to obtain insight into the propulsion-generating capacities of the internal foot joints. It is found that, next to a wide range of motion at the TC joint, substantial motion is observed at the TM and MP joint, underlining the importance of using a multi-segment foot model in primate gait analyses. More importantly, however, this study shows that although a compliant foot is less mechanically effective for push-off than a 'rigid' arched foot, it can contribute to the generation of propulsion in bipedal locomotion *via* stretch and recoil of the plantarflexor tendons and plantar ligaments.

Supplementary material available online at http://jeb.biologists.org/cgi/content/full/211/23/3661/DC1

Key words: biomechanics, energy-saving, mechanism, human evolution, joint movements, kinematics, primate locomotion.

INTRODUCTION

The fossil record and associated paleoenvironmental evidence (Harrison and Rook, 1997; Wolde Gabriel et al., 2001; Madar et al., 2002; Senut, 2003; Senut, 2006; Pickford, 2006) indicate that our early ancestors were tree-dwelling apes, and several evolutionary models (Stern, 1975; Prost, 1980; Tuttle, 1969; Tuttle, 1981; Senut, 2003; Senut, 2006; Clarke, 2003; Pickford, 2006) suggest bipedalism arose in this particular environment. The most recent model, based on observations of extended-leg bipedalism in wild orang-utans and supported by the fossil record (Thorpe et al., 2007; Crompton et al., 2008), suggests that habitual terrestrial bipedalism derived from arboreal hand-assisted bipedalism in a habitually orthograde hominoid. This ancestral orthogrady model (Crompton et al., 2008) is further supported by Filler (Filler, 2007), who found that a mutation(s) in homeobox genes governing lumbar vertebra morphology and facilitating habitual orthogrady, may have been present in our hominoid ancestors. This may well put back the origin of habitual bipedalism to earlier dates than currently held. The nature of this ancestral bipedal gait is still debated, but whether it was bent-hip, bent-knee (like gibbons and bonobos) (D'Août et al., 2002; Vereecke et al., 2006a) or stiff-legged (like orang-utans) (Thorpe et al., 2007), it was certainly executed with a relatively mobile, prehensile foot, and not with a foot like that of modern humans.

The modern human foot is highly specialized for terrestrial bipedalism. It has several unique characteristics, such as an enlarged calcaneal tuberosity, stabilized calcaneocuboid and talonavicular joints, a longitudinal arch and strong plantar aponeurosis (Harcourt-Smith and Aiello, 2004; Klenerman and Wood, 2006), all of which constitute the typical mechanical behaviour of the human foot during bipedalism. One of the most recognized features of the modern human foot is its ability to change from a compliant shock-absorber at heel-strike to a rigid lever at toe-off by supination of the subtalar joint (Donatelli, 1996). Further midfoot stabilization results from hallux dorsiflexion, tightening the plantar aponeurosis and offering the required stability for propulsion at push-off. This principle is known as the windlass mechanism (Hicks, 1954; Gershman, 1988; Fuller, 2000). In addition, the arched foot also enhances the efficiency of bipedalism by storage and release of elastic strain energy in the plantar aponeurosis (Ker et al., 1987). This dual function makes the modern human foot particularly well adapted for terrestrial, bipedal walking and running.

However, fossil evidence suggests that a truly 'modern' configuration of the human foot is a quite recent phenomenon, which evolved after the appearance of early *Homo* (approx. 1.8 Ma) (Kidd et al., 1996; Bramble and Lieberman, 2004; Harcourt-Smith and Aiello, 2004; Klenerman and Wood, 2006; Crompton et al., 2008), probably linked to long distance walking/running in a drier, more open environment. Some modern human-like features, such as an adducted hallux, increased metatarsophalangeal dorsiflexion and midfoot stabilization, may be found in earlier (5–2 Ma) hominin foot bones (see Harcourt-Smith and Aiello, 2004; Klenerman and Wood, 2006), but these

traits are not all present in any single early hominin foot, and combined with 'arboreal' characteristics, leading to a 'mosaic' foot structure with considerable mobility (Stern and Susman, 1983) (reviewed by Crompton et al., 2008). This implies that the adoption of a partially terrestrial bipedal gait – evidenced by the Laetoli footprints at ~3.5 Ma but possibly occurring as early as 6–7 Ma (Pickford et al., 2002; Richmond and Jungers, 2008) – predates the evolution of a specialised bipedal foot. Thus, our early hominin ancestors (>5 Ma) probably retained a relatively mobile and essentially flat foot structure, though frequently or even habitually, engaging in terrestrial bipedalism. This might mean that their behaviour still included arboreal activities (for which a mobile foot is advantageous), and/or that selective pressures for a terrestrially specialized foot were low. Though we might not yet fully understand the different evolutionary stages that led to the configuration of the modern human foot (mainly because of a lack of fossil foot bones) (Harcourt-Smith and Aiello, 2004), we can make inferences about the foot function of protohominins by studying the form and function of the foot in extant apes.

As an evaluative proxy for the foot function of protohominins, we have studied the foot function of untrained gibbons during terrestrial bipedal locomotion. Note that we are not claiming that gibbons are the best model for protohominins, nor that the architecture of the protohominin foot was similar to that of extant gibbons (claims which would be unsupported by fossil findings). Yet, the high mobility of the gibbon foot as well as the arboreal lifestyle and regular display of both arboreal and terrestrial bipedalism, makes the gibbon a valuable model for an ancestral tree-living hominoid/protohominin.

Gibbons are the most bipedal of all nonhuman primates, with bipedalism accounting for 10–12% of their locomotor activities (Cannon and Leighton, 1994). Gibbons alternate brachiation with fast bipedal bouts on large boughs and branches (diameter >10 cm) (Fleagle, 1976; Gittins, 1983), and bipedalism is their preferred terrestrial gait (more or less imposed by their long arms) when crossing gaps in the forest canopy (Sati and Alfred, 2002). This means that, despite the high incidence of brachiation, the hind limbs are important for propulsion generation in gibbons. Like most arboreal primates, gibbons have a mobile, prehensile foot structure with a divergent, opposable hallux. The gibbon foot is essentially flat (i.e. lacks a longitudinal arch as seen in modern humans) and displays a midtarsal break during bipedalism (Vereecke et al., 2003; DeSilva and MacLatchy, 2008). The plantar aponeurosis is relatively weakly developed compared with the human plantar aponeurosis (Vereecke et al., 2005b); however, other plantar connective tissues lying deep to the plantar aponeurosis, such as the plantar ligaments and the tendons of the digital flexors, are prominent (Vereecke et al., 2005b). Both the long digital flexors and gastrocnemius are short-fibred, pennate muscles, favouring economical force production and elastic energy usage. Unlike other nonhuman apes, the external portion of the gibbon Achilles' tendon (i.e. triceps surae tendon) is particularly long, comparable in size to the human Achilles' tendon. A diagram of potential elastic energy stores in the gibbon foot is given in Fig. 1.

The high tarsal mobility and absence of a longitudinal foot arch means that the gibbon foot cannot act as rigid lever for push-off; however, the muscle architecture of the lower limb lead us to hypothesise that the gibbon foot will contribute to the generation of propulsion *via* elastic recoil of plantarflexor tendons and plantar ligaments.

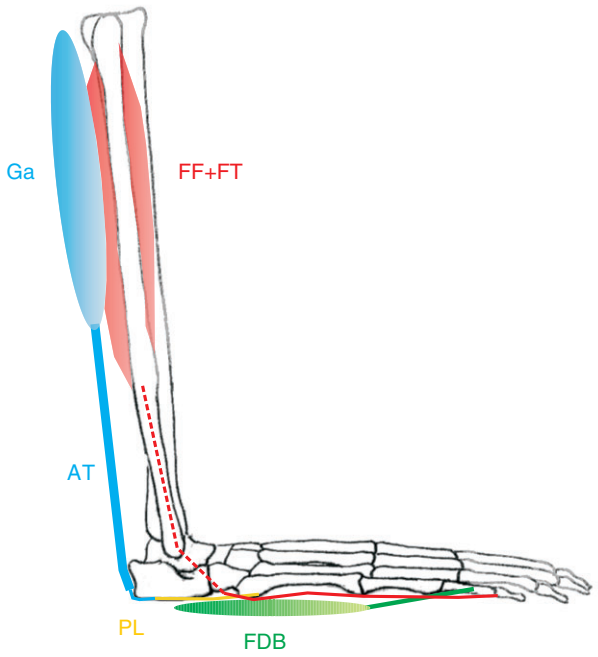

Fig. 1. Diagram of the gibbon foot indicating the major anatomical structures. Ga, gastrocnemius (part of the triceps); FF+FT, flexor fibularis and flexor tibialis (the long digital flexors); FDB, flexor digitorum brevis (the short digital flexors); PL, plantar ligaments; AT, Achilles' tendon.

MATERIALS AND METHODS

To evaluate these hypotheses, we have made a two-dimensional analysis of the internal joint mechanics of the foot during gibbon bipedalism using a four-link segment foot model. Available force and pressure data from a previous study (Vereecke et al., 2005a) are combined with detailed foot kinematics (this study) to calculate the external joint moments at the metatarsophalangeal, tarsometatarsal and talocrural joint during the stance phase. In addition, instantaneous joint power and external work are determined to obtain insight into the propulsion-generating capacities of the internal foot joints.

It must be emphasized that, in accordance with zoo policy, all bouts were collected without any direct interaction with the subjects. Though this ensures that all recorded bouts represent spontaneous bipedal walking, this constraint made data collection (since our camera was zoomed in on an area of 45 cm×45 cm, halfway along the wooden walkway) and analysis (manual digitization was necessary since subjects were unmarked) much more complicated and limited the number of successful trials that could be included in the analysis. Furthermore, practical considerations inherent to working with untrained animals in an unrestrained zoo environment meant that neither the setup in the present study, nor that used in an earlier force and pressure study by Vereecke et al. (Vereecke et al., 2005a) allowed for simultaneous recording of high-speed video and force/pressure measurements. Therefore, external joint moments were calculated by combining the registered point position data (collected in this study) with available force and plantar pressure data that had been collected simultaneously in a previous study (Vereecke et al., 2005a) using an AMTI force plate (Watertown, MA, USA) and a Footscan pressure mat (RSscan, Olen, Belgium).

Data acquisition

Sagittal joint motion was recorded during spontaneous bipedal locomotion of a group of white-handed gibbons (*Hylobates lar*, Linnaeus). Recording equipment was installed in the outdoor gibbon housing of the Wild Animal Park Planckendael (Belgium) and consisted of a high-speed MotionPro video camera (RedLake, Tucson, AZ, USA), set at sampling rate 250 Hz and shutter gate 1/500 s, mounted on a tripod, and positioned perpendicular to a 2 m-long wooden walkway and a 1 m-high wall reference-marked with a 0.1 cm×0.1 cm grid. The walkway was aligned orthogonally opposite a gateway to the indoor enclosure to enhance the frequency of spontaneous bipedal bouts, since no direct interaction with the animals was allowed by the zoo protocol. We collected a total of 68 bipedal bouts from three adult gibbons. All 68 records were used for qualitative evaluation and no apparent differences were observed in the footfall pattern and bipedal gait of the different individuals. For detailed analysis we have focused on recordings of a young male subject (6 years old; mass 6.3 kg) since owing to death from natural causes we were able to collect required anatomical data post-experimentally, and since ground reaction force profiles and plantar pressure distributions were available for this individual from a previous study (Vereecke et al., 2005a). Eight bipedal bouts of this individual were selected based on steadiness of overall walking speed (no apparent acceleration or deceleration), foot placement and stance phase duration. Only bouts with a stance phase duration between 0.50 and 0.65 s (corresponding to a speed range of ~0.7–1.0 m s^{-1}) and a nearly parasagittal (slight toe-out) foot position were retained. Comparison with digitized sequences of each of the other individuals indicated that the foot kinematics of the eight selected trials of the young male subject were indeed representative of the species' foot motion pattern. Quantitative foot motion data is presented only for this young adult male, but a figure of the footfall pattern of all three gibbons is provided to show the similarity in foot motion (Fig. 4).

Foot model

We developed a four-linked segment model of the lower hind limb using Kwon3D software (Kwon, 1994) to analyse the 2D motion of the talocrural, tarsometatarsal and metatarsophalangeal joints in the parasagittal plane. The different segments were defined by digitization of the following locations (Fig. 2): toe (T), metatarsophalangeal joint (MP), tarsometatarsal joint (TM), heel (H), talocrural (TC) and knee joint (K). Although these measurements were performed manually on each frame, the high resolution (1280 pixels×1024 pixels) of the full-frame video images enabled accurate digitization of the various points. To test repeatability of digitization, we digitized one sequence four times and calculated the standard deviation of the point positions. The standard deviation of the T, MP, TC, H and K position was ~4 mm, but, the standard deviation of the TM position amounted up to 6 mm. We therefore decided to determine the TM position using our knowledge of the subject's foot osteology – taken from the subject which had died after filming – rather than using manual digitizations. We used a Matlab routine (Matlab 7.2 for Windows) to calculate the position of the tarsometatarsal joint (TM) from the position of the heel (H) and talocrural joint (TC), based on the assumption that the hindfoot, enclosed by TC–TM–H, is a rigid triangle with known sides (see also Fig. 2). The length of the sides (TC–TM=26 mm, TC–H=35 mm, H–TM=39 mm) was obtained from measurements of the articulated foot skeleton of the deceased subject. This calculated position of the TM was used in all further analyses.

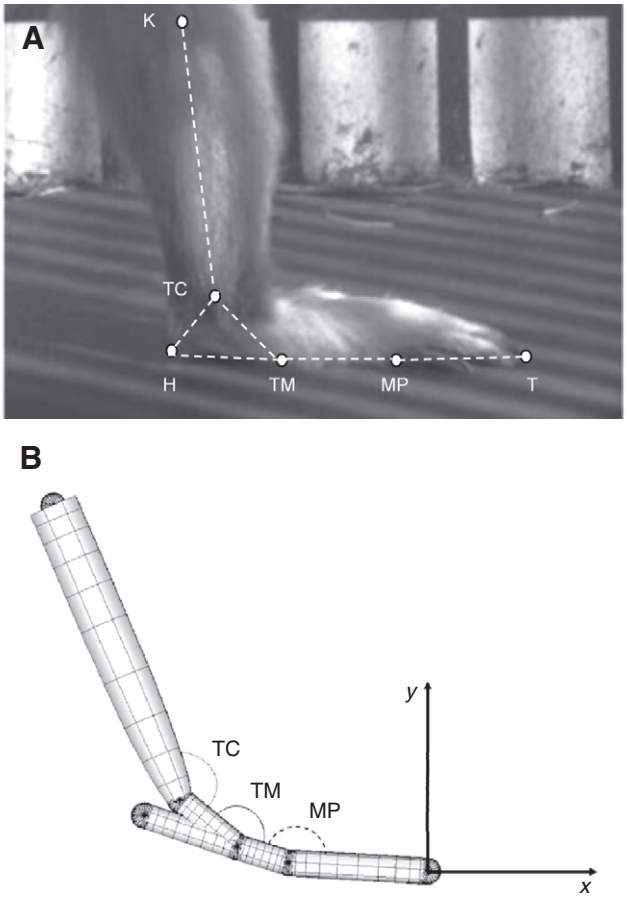

Fig. 2. The four-linked segment foot model. (A) Video image of the gibbon foot with indication of the digitized points. (B) Diagram of the joint angles. K, knee joint; TC, talocrural joint; H, heel; TM, tarsometatarsal joint; MP, metatarsophalangeal joint; T, toes.

The raw positional data were filtered using a fourth order Butterworth low-pass filter with 7 Hz cut-off frequency in Kwon3D. This was the optimal cut-off frequency, which was determined using residuals against frequency plots of the positional and angular data as described by Winter [(Winter, 1990) pp. 41–43]. In order to obtain the transformation parameters we digitized six points on the grid (0.2 m×0.1 m) of the reference wall in five consecutive frames of the camera view. An additional point, set at the tip of the toes, was used to translate the coordinate axes to the toe, T (0, 0). This calibration was done for each sequence because the camera position could change from sequence to sequence. Calibration was performed using the 2D-DLT Algorithm in KwonCC 3.01 for Windows (Kwon, 1994) and yielded a reconstruction error of 0.3–0.5 mm.

For generation of average point position data (x, y coordinates of T, MP, TM, TC and K) we resampled each sequence to comprise exactly 51 intervals of 2% stance phase duration (linear interpolation within the boundary measuring interval was applied; LabVIEW 8 for Windows). For each 2% interval the average point position (x, y coordinates; N=8) was calculated, and combined with the average forces ($\mathbf{F}_x$, $\mathbf{F}_y$) and centre of pressure (COP_x) data [taken from Vereecke et al. (Vereecke et al., 2005a)] which were also resampled to 51 intervals of 2% stance duration (see below). A Matlab routine was used to create stick figures of the position data and plot the

force vector (see below for origin of force information) over a full stance phase.

Joint angles

We computed three two-dimensional joint angles, at the talocrural (TC), tarsometatarsal (TM) and the metatarsophalangeal (MP) joints, from the point position data using basic trigonometry (Excel for Windows). The joint angles were defined as the angles between two adjacent segments, as illustrated in Fig. 2B. An increase in joint angle indicates joint plantarflexion; a decrease points to dorsiflexion. The joint angles were calculated for each sequence based on the resampled point coordinates (51 intervals) and the average joint angle of the eight sequences (± standard deviation) was plotted as a function of time.

External joint moments

The present dataset was carefully aligned with average force and pressure profiles from a previous study (Vereecke et al., 2005a). Integration of the force/pressure measurements and kinematics was performed by resampling each data set to 100% stance phase duration. Furthermore, in order to enable alignment of both data sets, the same reference frame, a right handed coordinate system with the toe as origin, was used. In Vereecke et al. (Vereecke et al., 2005a), the instantaneous centre of pressure (COP) was recorded using an RSscan pressure mat, installed on top of an AMTI force plate, and Footscan software was used to export the fore–aft coordinates of the COP (COP_x) during the full stance phase duration. We calculated the average vertical ($\mathbf{F}_y$) and horizontal ($\mathbf{F}_x$) force profile and the average path of the centre of pressure (COP_x; fore–aft component) for a series of bipedal sequences within the same speed range (~0.7–1.0 m s^{-1}), a nearly sagittal foot placement and performed by the same gibbon as the kinematic data collected in the current study.

Masses – and hence moments of inertia – of the foot segments are small; the total mass of the foot accounts for only 1.2% of the total body mass. This, combined with the limited linear and angular displacements (and hence accelerations) involved during stance, allowed for a static approach neglecting gravity and inertia. We computed the moments at the MP, TM and TC joint using a trigonometric method [cf. the FRFV approach of Winter [(Winter, 1990) pp. 92–93] (see also Biewener, 1983; Biewener, 1998; Hansen et al., 2004)]. As shown previously (Wells, 1981; Winter, 1990; Vaughan, 1996; Simonsen et al., 1997; Hansen et al., 2004) joint moments calculated with this method for the human ankle (and internal foot) joints, are very similar to those obtained from inverse dynamics calculations taking inertia and gravity into account.

For each 2% interval, this method calculates the moment arm (MA) of each joint (i.e. the perpendicular distance between the joint centre and the line of action of the resultant ground reaction force vector; GRF), which is then multiplied by the magnitude of the force vector [GRF=$\sqrt{}$($\mathbf{F}_x$^2+$\mathbf{F}_y$^2)] to yield the external joint moment. The sign of the external joint moment was defined according to the relative position of the *x*-coordinate of the MA–GRF intercept; when lying proximal to the joint (i.e. a smaller *x*-coordinate than that of the joint) it was considered negative (dorsiflexor moment), when distal to the joint (i.e. having a larger *x*-coordinate than that of the joint) it was considered positive (plantarflexor moment). The use of the trigonometric method with application of the resultant GRF at the COPx is in fact only justified for joints proximal to the point of application of that resultant force vector. However, from pressure distribution patterns (Fig. 3) (Vereecke et al., 2005a) it is obvious that foot segments situated distally to the one on which the resultant force applies (i.e. the location of the COP_x) are never loaded to a significant extent. This means that moments at joints distal to the COP_x are virtually zero (only gravity is in play). In practice, reliable estimates of joint moments can therefore be made for all foot joints throughout foot contact.

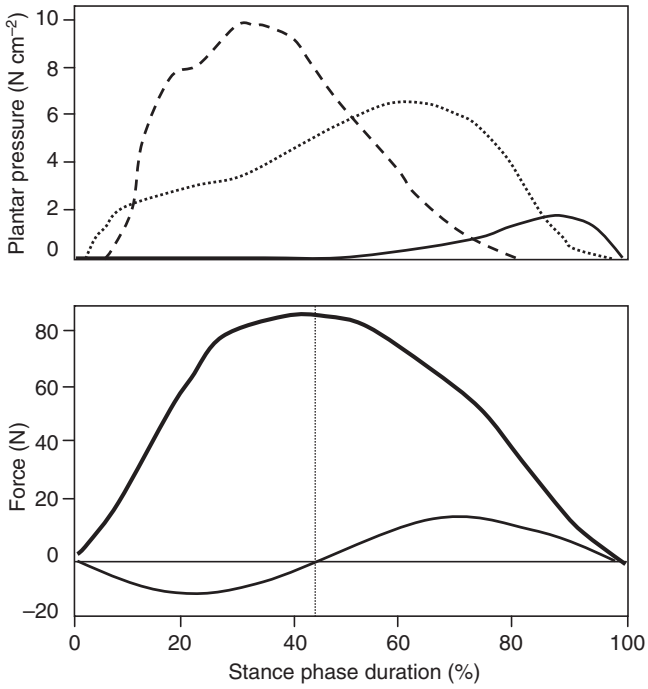

Fig. 3. Average plantar pressure (top) and force profile (bottom) against stance time (%) for the given gibbon subject [mass=6.3 kg; adapted from Vereecke et al. (Vereecke et al., 2005a; Vereecke et al., 2006b)]. The dashed line is the pressure under the TM joint (naviculare and M5 base), the dotted line is the pressure under the MP joint (metatarsal heads) and bold line is the pressure under the toes (distal phalanges). Bold line in force profile represents vertical force ($\mathbf{F}_y$), solid line represents horizontal force ($\mathbf{F}_x$).

Instantaneous joint power and external work

To estimate the potential elastic storage of energy in the triceps and digital flexors, we calculated instantaneous joint powers and positive and negative external work at each joint. The instantaneous power was obtained for each joint by multiplying joint moment (in N m) by angular joint velocity (in rad s^{-1}) during the stance phase. The joint moment and angular velocity used in these calculations are instantaneous values computed as averages of the joint moments and angular velocities occurring in the eight bouts. The instantaneous joint power was plotted as a function of stance phase duration (using a 12 ms time interval, corresponding to the previous 2% intervals), and the power–time integral was calculated to obtain positive and negative external work performed at each joint. Total foot power was also calculated, by summing the instantaneous joint powers of the MP, MT and TC joint, as well as positive and negative external work occurring at foot level. In this way potential energy transfer *via* multi-articular muscles and ligaments is considered.

RESULTS

Foot kinematics

Figs 4 and 5 illustrate the sagittal motion of the gibbon foot during the stance phase of a bipedal bout, which can be subdivided into

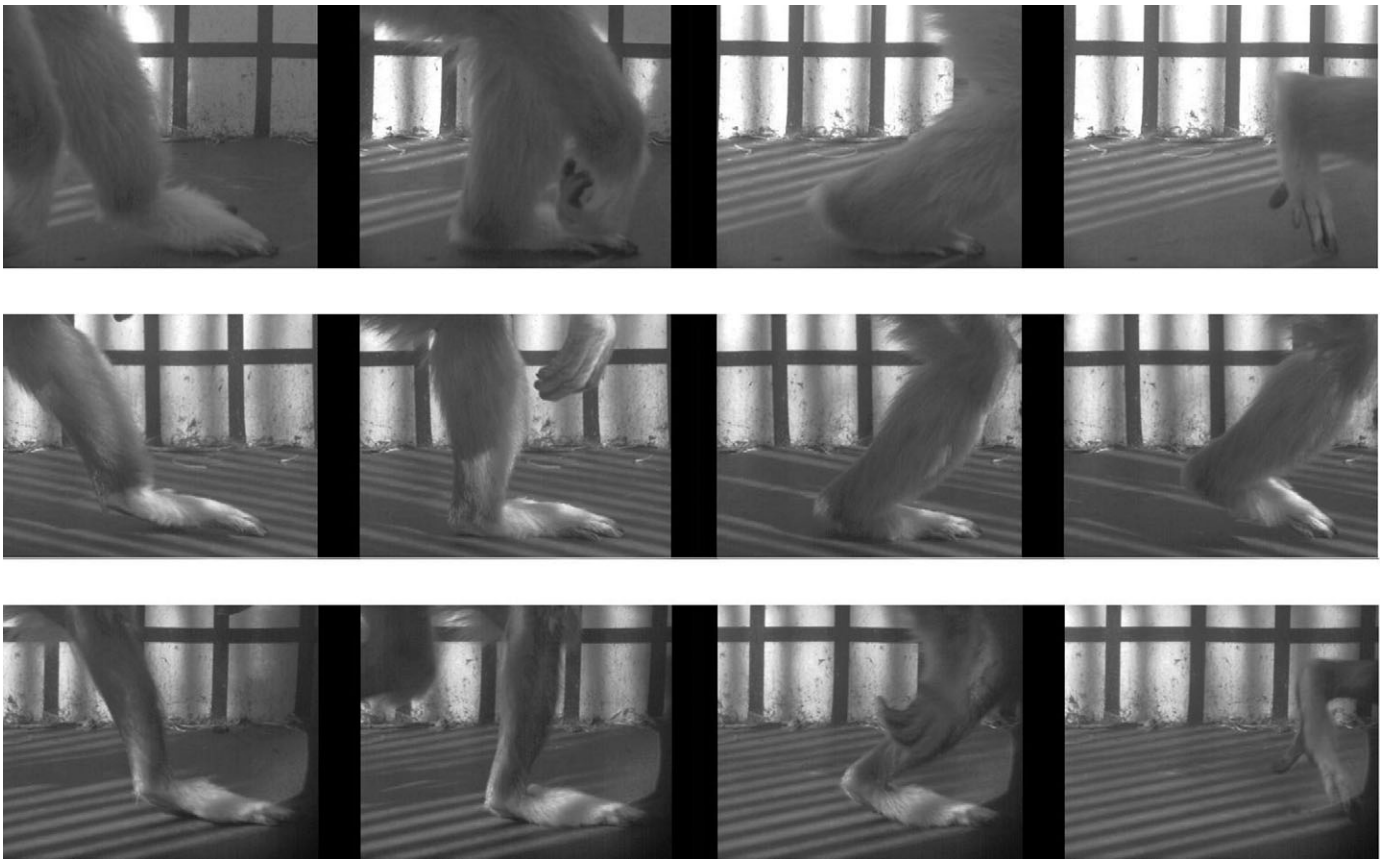

Fig. 4. Sagittal foot motion during the stance phase, demonstrating, from left to right, touchdown, loading, heel-rise and push-off. Shown are three representative bipedal bouts of three different individuals (top, young adult male; middle, adult male; bottom, adult female – note heel-elevated position during loading phase in the latter).

four phases with distinct kinematics and kinetics (see also Fig. S1 and Movies 1 and 2 in supplementary material).

The touchdown phase (0–10% stance phase)

Initial contact is made with forefoot or hallux, resulting in maximal ankle plantarflexion. Loading remains relatively low (<0.5 body mass; M_b).

The loading phase (10–50% stance phase)

During this predominantly braking phase (demonstrated by a negative horizontal force component, $\mathbf{F}_x$; cf. the posteriorly oriented GRF in Fig. 5B and Fig. 6), loading rises steadily until maximal weight bearing is achieved (~1.3 M_b). Peak pressures are located near the base of metatarsal V and the navicular bone (Fig. 6). Both the ankle and TM joint dorsiflex continuously, while no substantial motion occurs at the MP joint. The ground reaction force vector (GRF) is located distal to the TM joint (at metatarsal segment; Fig. 5B, Fig. 6).

The heel rise phase (50–80% stance phase)

This is a propulsive phase (demonstrated by a positive horizontal force component, $\mathbf{F}_x$; cf. the anteriorly oriented GRF in Fig. 5C and Fig. 6), with a forward shift of the GRF leading to peak pressures under the metatarsal heads. The GRF vector remains under the metatarsal segment during this phase (Fig. 5C, Fig. 6). The TC and TM joints continue to dorsiflex, reaching maximal dorsiflexion at the end of the heel-rise phase and leading to a continuous heel-rise while the forefoot remains on the ground.

The push-off phase (75–100% stance phase)

While loading drops (<0.8 M_b; unloading), the force shifts further forwards now leading to (small) peak pressures under the phalanges (Fig. 5D, Fig. 6). This phase is denoted by marked MP dorsiflexion (hyperextension) followed by MP plantarflexion, while the ankle and TM joint plantarflex until toe-off.

It should be noted that because of a high step-to-step variability in gibbons, the characteristics of these four phases can differ slightly between individuals and between steps. For example, in Fig. 4 it can be seen that during the loading phase the foot can either have a heel-down or a heel-elevated position, though the latter was only observed sporadically.

Joint angles

The MP joint remains in a neutral (180 deg.) or slightly flexed position throughout the first 80% of the stance phase, while there is a variable degree of dorsiflexion at the TM joint (Fig. 7). Heel rise is associated with dorsiflexion at the TM (and TC) joint, so that the forefoot remains in contact with the substrate while the heel is off the ground. This heel rise event is followed by dorsiflexion at the MP joint (around 75% of the stance phase), and TM joint plantarflexion.

The range of motion at the TM and MP joint averages 38 deg. and 28 deg., respectively, and the joint motions are characterized by a strong angular displacement during the last 20% of the stance phase. The largest movement occurs, however, at the TC joint, which dorsiflexes continuously until ~80% of the stance phase (apart from some initial plantarflexion) as the tibia rotates over the foot (Fig. 5).

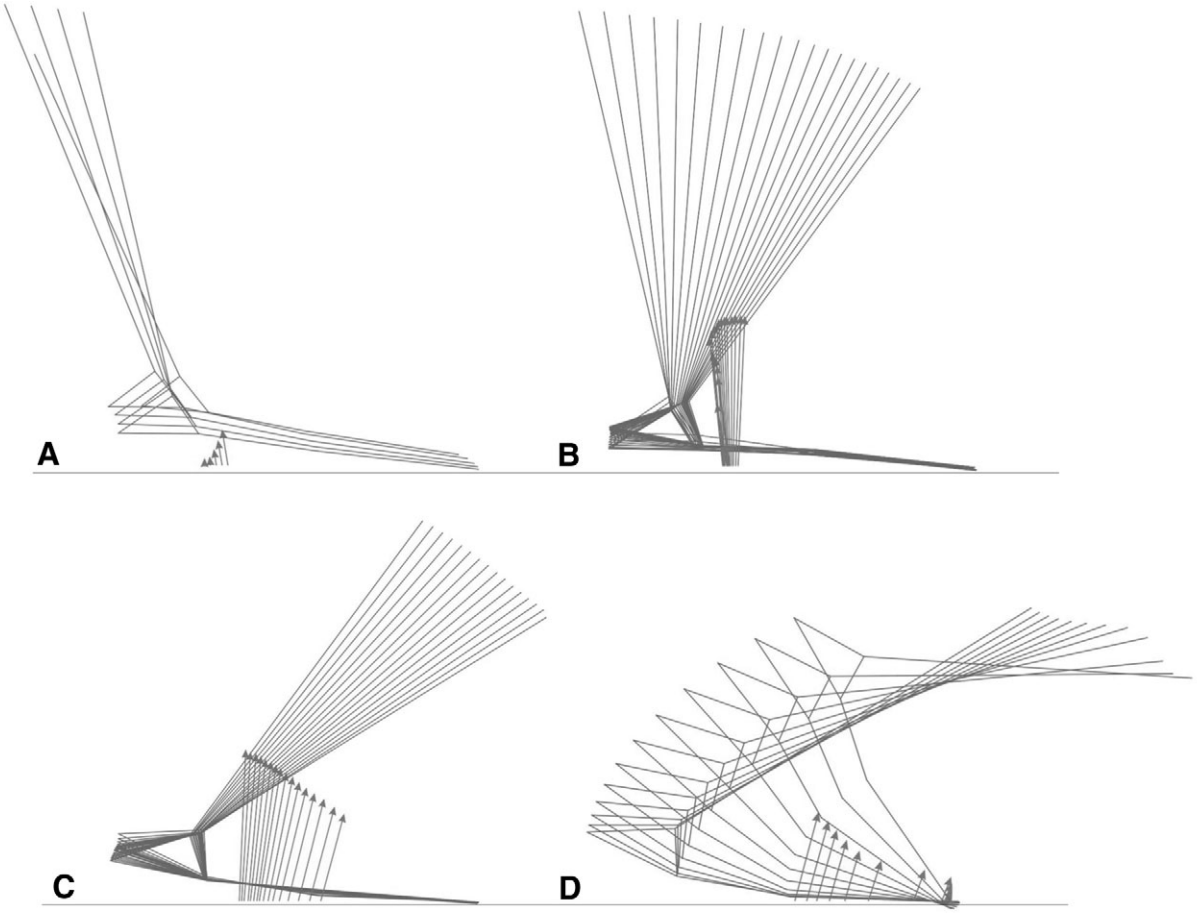

Fig. 5. Stick figure of an average stance phase showing the four-segment link foot model and the ground reaction force vector. (A) Touchdown (0–10% stance phase), (B) loading phase (10–50% stance phase), (C) heel-rise (50–80% stance phase), and (D) push-off (80–100% stance phase); see text for details. [Note that the initial contact (0–10% stance phase) is typically made with a widely abducted hallux, not with the hindfoot (H–TM segment) although this illustration and Fig. 6 do not give this impression.]

The total range of motion at the TC joint averages 71 deg. during the stance phase. The TC joint plantarflexes slightly during the last 20% of the stance phase and continues to plantarflex during early swing.

External joint moments

The joint moments at the TC and TM joint are positive throughout the stance phase, pointing to a continuous plantarflexor moment (Fig. 7). This results from the fact that the GRF vector runs anterior to both joints at all times (Fig. 5), forcing the joints into dorsiflexion and leading to a counteracting plantarflexor moment presumably generated by the plantarflexor muscles (triceps surae and long digital flexors). As explained before, virtually no moments occur at the MP joint as long as the phalangeal segments remain unloaded (Figs 3 and 5). Therefore, only during the last 20% of the stance phase, when the phalanges are clearly loaded, do we observe a (positive) plantarflexor moment at the MP joint, presumably generated by the long digital flexors and intrinsic plantar foot muscles.

Instantaneous joint power and external work

Although the external joint moments indicate to a certain extent which muscle groups (flexors, extensors) are active, net joint moments cannot reveal co-contractions and antagonists. However, net joint powers and external work can be used to gain insight into the manner in which these muscle groups function throughout the contact phase of the step cycle: generating or absorbing mechanical energy (i.e. concentric *versus* eccentric contractions). In addition, it allows us to evaluate the potential for elastic energy storage in the muscle–tendon units crossing these joints. Instantaneous joint power and external work performed at each joint are presented in Fig. 8.

During the first 80% of the stance phase, the TC joint dorsiflexes while there is a plantarflexor moment, resulting in the generation of negative power and negative external work (–2.15 J). While still having a plantarflexor moment, the TC joint plantarflexes during the final 20% of the stance phase, generating positive power and positive external work (+0.40 J). Thus, if the plantarflexors are activated, eccentric contraction is followed by concentric contraction in late stance. A similar action is found for the TM joint, with negative power and external work production (–0.37 J) during the first 70% of the stance phase, and positive power and external work (+0.40 J) performed during the last 30%. At the MP joint there is no power output (or dorsiflexion) during the first 80% of the stance phase as joint moments are zero. However, as the MP joint dorsiflexes during 80–90% of the stance phase, there is negative power and negative external work production (–0.05 J) and hence eccentric contraction of the digital flexors (assuming activation). During the last 10% of the stance phase, the MP joint plantarflexes, yielding some positive power and external work (+0.12 J) by concentric contraction of the digital flexors.

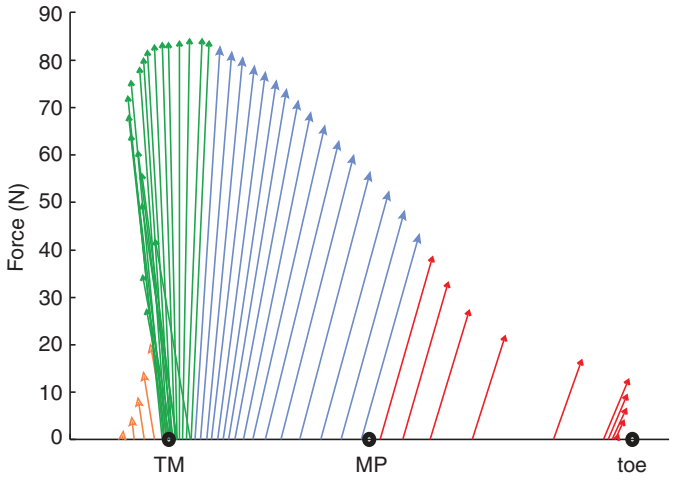

Fig. 6. Butterfly (Pedotti) diagram illustrating the ground reaction force vectors as a function of foot length. The colours of the arrows indicate timing: orange arrows, 0–10% stance phase; green arrows, 10–50%; blue arrows, 50–80%; and red arrows, 80–100%. TM, tarsometatarsal joint; MP, metatarsophalangeal joint. Arrows pointing to the left denote braking, arrows pointing to the right denote acceleration.

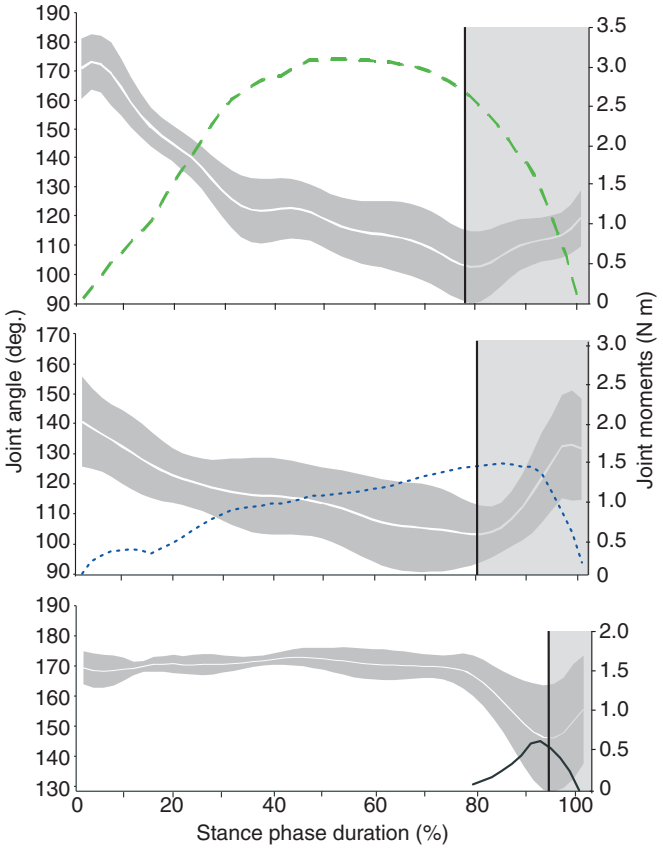

Fig. 7. Combination of average joint angles (white line; grey shaded area indicates standard deviation) and moments at the TC (top, dashed line), TM (middle, dotted line) and MP(bottom, solid line) joints against stance time (%). Plantarflexor moments are positive, dorsiflexor moments negative; a decreasing angle means dorsiflexion, an increase points to plantarflexion. Shaded areas on the right denote positive power output (i.e. plantarflexor moment×joint plantarflexion).

However, whereas the triceps only crosses the TC joint, the long digital flexors cross the TC, TM and MP joint and the short digital flexors cross both the TM and MP joint (see Fig. 1). This anatomical configuration means that energy transfer *via* the digital flexors is possible across the three joints. To account for this, we have added up the power profiles of the three joints (Figs 8 and 9). The estimated external work performed at foot level amounts to –2.43 J during the first 80% of the stance phase and +0.78 J during the last 20%. Scaled to body mass (6.3 kg) and average stride length (0.65 m), this gives $-1.25\,\mathrm{J\,kg^{-1}\,m^{-1}}$ energy absorption and $+0.20\,\mathrm{J\,kg^{-1}\,m^{-1}}$ energy output.

DISCUSSION

This aim of this work was to provide insight in the mechanics of the gibbon foot during terrestrial bipedalism. It investigated primarily whether leg muscles and connective tissue structures on the plantar aspect of the foot can contribute to propulsion *via* elastic recoil or whether they are a source of mechanical energy loss. A four-segment planar foot model was judged most appropriate for this study, as ankle joint motion during bipedalism occurs predominantly along the sagittal plane (Vereecke et al., 2005a) [cf. humans (Belli et al., 2002; Hansen et al., 2004)] – despite some abduction/adduction and pronation/supination – and the combined rotations of the digits at the TM and MP joints also occur about a near-transverse axis.

Foot joint mechanics during bipedalism

Gibbons have a very flexible foot structure, where a passive range of motion of ~150 deg. at the TC and MP joints can be demonstrated by manipulation of cadaveric feet (personal observation). This high joint mobility is definitely related to their habitual locomotor and postural behaviour. Wild gibbons are confined to life in the trees, and the mobile ankle and foot joints provide the agility needed to adjust to the varying inclination, orientation and size of branches in this complex 3D environment (Gebo, 1993). The long, curved toes, abducted hallux, strong flexors and mobile tarsal joints of the gibbon foot facilitate a powerful grip, which is beneficial during climbing, clambering and quadrumanous hanging (Fleagle, 1999). As one would expect, this mobility is also present during bipedalism (see also Fig. S1 and Movies 1 and 2 in supplementary material), and means that the gibbon foot cannot act as a rigid lever during push-off. This high foot mobility also underlines the importance of using a multi-segment foot model in the analysis of gibbon, and ultimately primate, locomotion.

Despite the larger angular excursion of the TC and TM joints in gibbon (71 deg. and 38 deg., respectively) compared to human bipedalism (15–25 deg. and 10–15 deg., respectively), the shape of the joint angle profiles is largely similar in both species (Kidder et al., 1996; Carson et al., 2001; MacWilliams et al., 2003). The TC and TM joints dorsiflex during the first 80% of the stance phase and plantarflex during the last 20% (Fig. 7). In gibbon bipedalism there is no initial TC plantarflexion, however, as gibbons touchdown with the forefoot (hallux or metatarsal heads; Fig. 4) and not with the heel, like other apes and humans (i.e. absence of a heel-strike) (Schmitt and Larson, 1995; Vereecke et al., 2005a). As soon as the digits touch down the tendons of the long digital flexors will be stretched since the long digital flexors are relatively short muscle tendon units in gibbons (passive extension of the digits is only possible when the TC joint is plantarflexed and TC joint dorsiflexion is coupled with flexion of the digits). Thus, eccentric work and potential energy storage at the TC and TM joints can start from

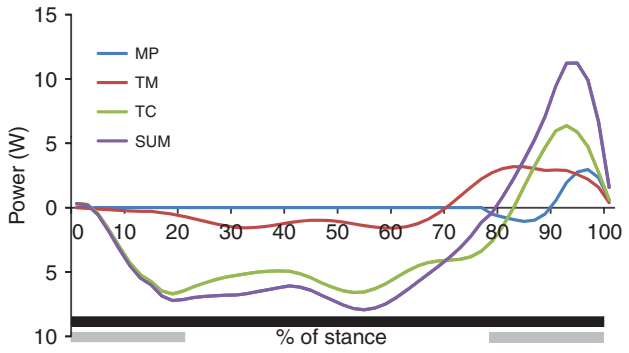

Fig. 8. Instantaneous powers performed at the MP, TM and TC joints and the total foot power (SUM) during stance. The bars at the bottom indicate foot contact of the stance foot (black) and contralateral foot (grey).

initial contact. This tightening of the tendons of the long digital flexors might also be responsible for the coupling of TM plantarflexion and MP dorsiflexion in late stance, something which is also observed in human gait (Carson et al., 2001). Dorsiflexion at the MP joint is, however, more pronounced in humans than in gibbons: 35–45 deg. *vs* 28 deg. (Kidder et al., 1996; Carson et al., 2001; MacWilliams et al., 2003). This marked toe dorsiflexion is a typical feature of human gait, reflected in the dorsal expansion of the MP joint articulation, and plays an important role in the windlass mechanism (i.e. tightening of the longitudinal foot arch by winding the plantar fascia around the metatarsal heads) (Gershman, 1988; Fuller, 2000).

The joint moment profile of the TC joint during gibbon bipedalism, and specifically the plantarflexor moment during the entire stance phase duration, corresponds to previous results reported by Ishida et al. (Ishida et al., 1976). It is similar to the human pattern but is considerably smaller in magnitude when scaled to body mass and foot length (0.29 in gibbons *vs* 0.54 in humans). Ishida et al. (Ishida et al., 1976) suggested that the presence of a plantarflexor moment prior to toe-off points to an active push-off in gibbons, a finding supported by their EMG results showing maximal activation of the triceps surae during late stance (see also Okada and Kondo, 1982). However, their EMG data show that during gibbon bipedalism the long digital flexors are also active throughout stance. Combined with our results, this suggests that, during late stance, co-contraction of the triceps and long digital flexors will lead to plantarflexion at both TC and TM joints, generating propulsion for push-off. Contraction of the digital flexors will also lead to plantarflexion at the MP joint during the last 10% of stance, but given the small plantarflexion moment the contribution of the MP joint to propulsion will be small.

Potential for elastic storage

Instantaneous joint powers were calculated to get insight in the function of the recruited muscle groups during the stance phase. The results show that during the first 70–80% of the stance phase, the plantarflexor muscles work eccentrically, potentially loading the well-developed Achilles' tendon, long digital flexor tendons and connective tissue components of the plantar foot (cf. Vereecke et al., 2005b) with elastic energy. This is followed by concentric contraction of the plantarflexor muscles during late stance. The amount of positive external work performed at the TC and TM joint is similar, and is preceded by generation of negative external work at both joints (Fig. 8). To estimate how much of this positive external work could come from elastic recoil, we compared the relative amounts of negative and positive work at both joints during stance. We took account of the criteria suggested by Gregersen and colleagues (Gregersen et al., 2007), namely, (1) positive work should be preceded by negative work (otherwise no elastic energy could have been stored), (2) the plantarflexor muscles must be active and exerting force throughout stance [confirmed by a continuous plantarflexor moment at each joint (Fig. 7) and EMG data (Ishida et al., 1976; Okada and Kondo, 1982)], and (3) at each joint plantarflexion should not exceed the amount of dorsiflexion (confirmed by the calculated joint angles; Fig. 7). Our estimates indicate that 100% of the positive work performed at the TC joint, and 90% of that performed at the MT joint could, in theory, come from elastic recoil. We can therefore conclude that plantarflexor muscle–tendon systems crossing the TC and TM joints (Achilles' tendon and tendons of the long digital flexors) can function as springs during hylobatid bipedalism, storing and releasing elastic energy with each step. Yet, the importance of this recoil for the cost of bipedal locomotion must be discussed.

To get an idea about the contribution of the positive external work performed at the foot to whole body propulsion, we compared the power profiles of the foot joints to those calculated from fluctuations of the centre of mass (COM) in an earlier publication (Vereecke et al., 2006b). The positive external work generated at the foot joints (+0.78 J) amounts to around 54% of the positive external muscular work (+1.45 J) delivered at COM-level during stance (Fig. 9) suggesting a substantial contribution. If we look at the relative timing, however, the foot joints obviously generate positive power whereas power at COM-level is negative (Fig. 9), suggesting that tendon recoil (at foot level) does not contribute to whole-body dynamics. However, power calculations based on COM fluctuations overlook the work performed by the individual limbs during double support, as these have an opposing action. As shown for human walking (Bastien et al., 2003; Donelan et al., 2002), the leading leg performs predominantly negative work, whereas the trailing leg performs positive work during double support. It seems probable, therefore, that the positive work output at the level of the foot can still contribute substantially to countering the braking action of the contralateral (leading) limb. This is further supported by the observation that the positive work performed at foot level coincides with the upward movement of the COM (the COM position is highest during double stance and lowest during midstance; cf. human running) (Vereecke et al., 2006b).

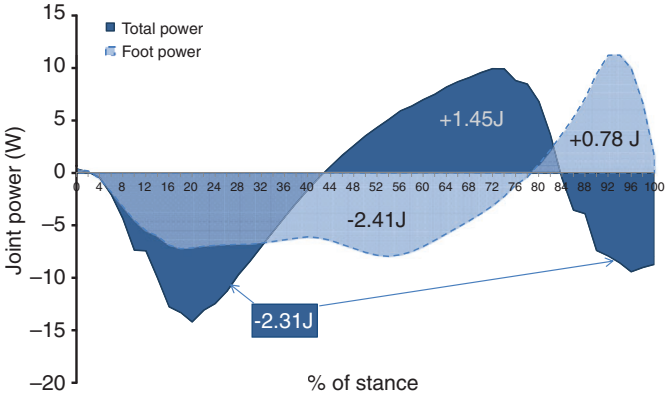

Fig. 9. Power performed at the foot (sum of MP, TM and TC joint power; light blue) and total power performed to move the centre of mass (dark blue) during stance with estimates of positive and negative external work.

In human bipedalism, stretch and recoil of the Achilles' tendon leads to an energy recovery of ~35% (Alexander, 1991b), which is further increased to 52% by flattening of the longitudinal foot arch and resulting stretching of the extensive plantar aponeurosis and plantar ligaments (Ker et al., 1987). Quite unexpectedly, both recovery mechanisms are also present in gibbon bipedalism. Instead of a flattening of the longitudinal arch, as seen in human walking and running (Ker et al., 1987), the flat and mobile gibbon foot bends during the stance phase [predominantly at the TM joint, i.e. the so-called 'midtarsal break' (Vereecke et al., 2003; DeSilva and MacLatchy, 2008)], potentially storing elastic strain energy in the stretched plantar tendons and ligaments. Such a 'reversed arch' mechanism has previously been described by Bennett and colleagues in a study on cadaveric feet of monkeys [vervet monkeys and macaques (Bennett et al., 1989; Alexander, 1991a)]. They identified the long and short plantar ligament and the calcaneonavicular/spring ligament as potential sources of elastic energy storage in the primate foot (see also Bennett et al., 1989). However, our results indicate that the relatively strong tendons of the digital flexors (Vereecke et al., 2005b; Payne et al., 2006) which run at the plantar side of the foot, will be even more important energy stores.

From prehensile tool to efficient lever

In an arboreal setting a flexible foot structure is essential, allowing a powerful grip in a wide range of locomotor modes and postures (e.g. the dorsiflexed-supinated foot position in climbing). Considering the arboreal origin of primates, it is not surprising that most extant nonhuman primates have flexible feet, and even the foot of humans, obligate terrestrialists, bears hallmarks of an arboreal ancestry (e.g. the organization of the intrinsic foot muscles, the variable amount of hallux abductability, and modified sellar-shape of the talar trochlea) (Lewis, 1980). In terrestrial locomotion, however, a flexible foot structure is less favourable than a 'rigid' foot as it has a reduced capacity for generation of propulsion. This is evident in the force profiles of gibbon bipedalism (Fig. 6), which lack the sudden drop of the vertical force at terminal stance associated with a strong push-off. Such clear propulsive push-off has not been observed in any of the living apes and seems to be a unique human feature, related to the rigidity of the human foot in terminal stance (Li et al., 1996; Crompton et al., 2008).

The change in foot structure from apes and early hominins to modern humans is clearly induced by a shift from slow, arboreal to faster, terrestrial locomotion. The occurrence of pedal modifications associated with terrestrial cursoriality is certainly not unique to humans; textbook examples include the specialized foot/hand and limb structure of cursorial mammals. Ungulates (e.g. horses, giraffes) and carnivores (e.g. wolves, cheetahs) are extreme examples hereof, characterized by elongated distal limb segments, tarsus and metatarsus, reduced distal limb mass, joint motion restricted to the parasagittal plane, and digitigrade or even unguligrade foot/hand posture (Hildebrand, 1995). Similar modifications in foot structure and posture have also evolved in the most committed terrestrial primates: patas monkeys, baboons, geladas (e.g. elongated legs, long metacarpals/tarsals and relatively short digits, straight phalanges, digitigrade or semi-plantigrade foot/hand posture, reduced hallux/pollex) (Ankel-Simons, 1999; Polk, 2002; Jungers et al., 2005; Lemelin and Schmitt, 2007) and humans. According to Bramble and Lieberman (Bramble and Lieberman, 2004), nine structures in the human foot can be considered as cursorial adaptations, including: a stabilized plantar arch, powered and stabilized plantarflexion, enlarged calcaneal tuberosity, close-packed calcaneocuboid joint, permanently adducted hallux, short toes and distal mass reduction. Most of these changes lead to increased stiffness/rigidity and enhanced mechanical leverage of the human foot, yet without sacrificing its essentially plantigrade and arboreal configuration which makes it a truly unique structure.

Changes in pedal morphology will only occur if they provide a strong selective advantage (e.g. improved speed and/or reduced locomotor cost), which lets us postulate that the specialized modern human foot could only have evolved in a predominantly terrestrial and cursorial hominin as it provides a clear benefit in fast terrestrial locomotion yet will compromise arboreal locomotion (especially fine-branch habitat). However, since the acquisition of a bipedal gait probably arose in an arboreal setting, and preceded the adoption of an obligate terrestrial lifestyle, the feet of early hominins probably remained quite flat and flexible until ~4 Ma (Stern and Susman, 1983; Harcourt-Smith and Aiello, 2004; Gebo and Schwartz, 2006) and might have displayed a midtarsal break during bipedalism. Such a midtarsal break, or high midfoot flexibility, is reported for gibbons, chimpanzees and bonobos (Bojsen-Møller, 1979; D'Août et al., 2002; Vereecke et al., 2003; Vereecke and Van Sint Jan, 2008; DeSilva and MacLatchy, 2008), and allows the heel to rise while the metatarsals and phalanges remain on the ground. As shown in this paper, this midfoot dorsiflexion will stretch the tendons and ligaments running across the plantar side of the foot, potentially storing elastic energy and eventually contributing to propulsion generation at push-off.

To sum up, this study indicates that although a compliant arboreally adapted foot is less mechanically effective for push-off than a 'rigid' arched foot, it can contribute to propulsion generation in bipedalism *via* stretch and recoil of the plantarflexor tendons and plantar ligaments.

LIST OF ABBREVIATIONS

COP_x	*x*-component of the centre of pressure
GRF	ground reaction force
H	heel
$\mathbf{F}_x$	horizontal component of force vector
$\mathbf{F}_y$	vertical component of force vector
K	knee
Ma	megaannum or 1 million years
MA	moment arm
M_b	body mass
MP	metatarsophalangeal
T	toe
TC	talocrural
TM	tarsometatarsal

The authors wish to thank Professor Robin H. Crompton, Dr Todd Pataky, Paolo Caravaggi, and the zookeepers of the Wild Animal Park Planckendael for their helpful contribution, and the anonymous reviewers for their valuable comments on the original manuscript. This work was supported by a research fellowship from the Fund for Scientific Research, Flanders, by an International Joint Project from the Royal Society, and by the Flemish Government through structural support to the Centre for Research and Conservation (RZSA, Belgium).

REFERENCES

Alexander, R. M. (1991a). Elastic mechanisms in primate locomotion. *Z. Morphol. Anthropol.* **78**, 315-320.
Alexander, R. M. (1991b). Energy-saving mechanisms in walking and running. *J. Exp. Biol.* **160**, 55-69.
Ankel-Simons, F. (1999). *Primate Anatomy: An Introduction*. New York: Academic Press.
Bastien, G. J., Heglund, N. C. and Schepens, B. (2003). The double contact phase in walking children. *J. Exp. Biol.* **206**, 2967-2978.
Belli, A., Kyrolainen, H. and Komi, P. V. (2002). Moment and power of lower limb joints in running. *Int. J. Sports Med.* **23**, 136-141.
Bennett, M. B., Ker, R. F. and Alexander, R. M. (1989). Elastic strain energy storage in the feet of running monkeys. *J. Zool.* **217**, 469-475.
Biewener, A. A. (1983). Allometry of quadrupedal locomotion: the scaling of duty factor, bone curvature and limb orientation to body size. *J. Exp. Biol.* **105**, 147-171.
Biewener, A. A. (1998). Muscle–tendon stresses and elastic energy storage during locomotion in the horse. *Comp. Biochem. Physiol. B* **120**, 73-87.

Bojsen-Møller, F. (1979).Calcaneocuboid joint and stability of the longitudinal arch of the foot at high and low gear push off. *J. Anat.* **129**, 165-176.
Bramble, D. M. and Lieberman, D. L. (2004). Endurance running and the evolution of Homo. *Nature* **432**, 345-352.
Cannon, C. H. and Leighton, M. (1994). Comparative locomotor ecology of gibbons and macaques: selection of canopy elements for crossing gaps. *Am. J. Phys. Anthropol.* **93**, 505-524.
Carson, M. C., Harrington, M. E., Thompson, N., O'Connor, J. J. and Theologis, T. N. (2001). Kinematic analysis of a multi-segment foot model for research and clinical applications: a repeatability analysis. *J. Biomech.* **34**, 1299-1307.
Clarke, R. J. (2003). Bipedalism and arboreality in *Australopithecus*. *Cour. Forsch.-Inst. Senckenberg* **243**, 79-83.
Crompton, R. H., Vereecke, E. E. and Thorpe, S. K. S. (2008). Locomotion and posture from the common hominoid ancestor to fully modern hominins, with special reference to the last common panin/hominin ancestor. *J. Anat.* **212**, 501-543.
D'Août, K., Aerts, P., De Clercq, D., De Meester, K. and Van Elsacker, L. (2002). Segment and joint angles of hind limb during bipedal and quadrupedal walking of the bonobo (*Pan paniscus*). *Am. J. Phys. Anthropol.* **119**, 37-51.
DeSilva, J. M. and MacLatchy, L. M. (2008). Revisiting the midtarsal break. *Am. J. Phys. Anthropol.* **135**, S46; 89.
Donatelli, R. A. (1996). *The Biomechanics of the Foot and Ankle*. 2nd edn. Philadelphia: F.A. Davies.
Donelan, J. M., Kram, R. and Kuo, A. D. (2002). Mechanical work for step-to-step transitions is a major determinant of the metabolic cost of human walking. *J. Exp. Biol.* **205**, 3717-3727.
Filler, A. (2007). Homeotic evolution in the Mammalia: diversification of Therian axial seriation and the morphogenetic basis of human origins. *PLoS ONE* **2**, e1019.
Fleagle, J. G. (1976). Locomotion and posture of the Malayan siamang and implications for hominid evolution. *Folia Primatol.* **26**, 245-269.
Fleagle, J. G. (1999). *Primate Adaptation and Evolution*. 2nd edn. New York: Academic Press.
Fuller, E. A. (2000). The windlass mechanism of the foot-a mechanical model to explain pathology. *J. Am. Podiatr. Med. Assoc.* **90**, 35-46.
Gebo, D. L. (1993). Functional morphology of the foot in primates. In *Postcranial Adaptation in Nonhuman Primates* (ed. D. L. Gebo). DeKalb: Northern Illinois University Press.
Gebo, D. L. and Schwartz, G. T. (2006). Foot bones from Omo: implications for hominid evolution. *Am. J. Phys. Anthropol.* **129**, 499-511.
Gershman, S. (1988). A literature review of midtarsal joint function. *Clin. Podiatr. Med. Surg.* **5**, 385-391.
Gittins, P. S. (1983). Use of forest canopy by the agile gibbon. *Folia Primatol.* **40**, 134-144.
Gregersen, C. S., Silverton, N. A. and Carrier, D. R. (2007). External work and potential for elastic energy storage at the limb joint of running dogs. *J. Exp. Biol.* **201**, 3197-3210.
Hansen, A. H., Childress, D. S., Miff, S. C., Gard, S. A. and Mesplay, K. P. (2004). The human ankle during walking: implications for design of biomimetic ankle prostheses. *J. Biomech.* **37**, 1467-1474.
Harcourt-Smith, W. E. H. and Aiello, L. C. (2004). Fossils, feet and the evolution of human bipedal locomotion. *J. Anat.* **204**, 403-416.
Harrison, T. and Rook, L. (1997). Enigmatic anthropoid or misunderstood ape? The phylogenetic status of *Oreopithecus bambolii* reconsidered. In *Function, Phylogeny, and Fossils: Miocene Hominoid Evolution and Adaptations* (ed. D. R. Begun, C. V. Ward and M. D. Rose), pp. 327-362. New York: Plenum Press.
Hicks, J. H. (1954). The mechanics of the foot: II. the plantar aponeurosis and the arch. *J. Anat.* **88**, 25-30.
Hildebrand, M. (1995). *Analysis of Vertebrate Structure.* 4th edn. New York: Wiley.
Ishida, H., Kimura, T., Okada, M. and Yamazaki, N. (1976). Kinesiological aspects of bipedal walking in gibbons. *Gibbon Siamang* **4**, 135-145.
Jungers, W. L., Lemelin, P., Godfrey, L. R., Wunderlich, R. E., Burney, D. A., Simons, E. L., Chatrath, P. S., James, H. F. and Randria, G. F. (2005). The hands and feet of Archaeolemur: metrical affinities and their functional significance. *J. Hum. Evol.* **49**, 1, 36-55.
Ker, R. F., Bennett, M. B., Bibby, R. S., Kester, R. C. and Alexander, R. M. (1987). The spring in the arch of the human foot. *Nature* **325**, 147-149.
Kidd, R. S., O'Higgins, P. and Oxnard, C. E. (1996). The OH8 foot: a reappraisal of the hindfoot utilizing a multivariate analysis. *J. Hum. Evol.* **31**, 269-291.
Kidder, S. M., Abuzzahab, F. S. J., Harris, G. F. and Johnson, J. E. (1996). A system for the analysis of foot and ankle kinematics during gait. *IEEE Trans. Rehabil. Eng.* **4**, 25-32.
Klenerman, L. and Wood, B. (2006). *The Human Foot: A Companion to Clinical Studies*. Heidelberg: Springer.
Kwon, Y.-H. (1994). Kwon 3D Motion Analysis Package 2.1, User's reference manual. V-TEK Corporation. Korea: Anyang.
Lemelin, P. and Schmitt, D. (2007). Origins of grasping and locomotor adaptations in primates: comparative and experimental approaches using an opossum model. In *Primate Origins: Adaptations and Evolution* (ed. M. J. Ravosa and M. Dagosto), pp. 329-380. New York: Springer.
Lewis, O. J. (1980). The joints of the evolving foot: part 1, the ankle joint. *J. Anat.* **130**, 527-543.
Li, Y., Crompton, R. H., Alexander, R. M., Gunther, M. M. and Wang, W. J. (1996). Characteristics of ground reaction forces in normal and chimpanzee-like bipedal walking by humans. *Folia Primatol.* **66**, 137-159.
MacWilliams, B. A., Cowley, M. and Nicholson, D. E. (2003). Foot kinematics and kinetics during adolescent gait. *Gait Posture* **17**, 214-224.
Madar, S. I., Rose, M. D., Kelley, J., MacLatchy, L., Pilbeam, D. (2002). New Sivapithecus postcranial specimens from the Siwaliks of Pakistan. *J. Hum. Evol.* **42**, 705-752.
Okada, M. and Kondo, S. (1982). Gait and EMG during bipedal walk of a gibbon (*Hylobates agilis*) on flat surface. *J. Anthrop. Soc. Nippon* **90**, **3**, 325-330.
Payne, R. C., Crompton, R. H., Günther, M. M., D'Août, K., Savage, R., Isler, K. and Vereecke, E. (2006). Morphological analysis of the hindlimb in apes and humans. Part I: Muscle Architecture. *J. Anat.* **208**, 709-724.
Pickford, M. (2006). Paleoenvironments, paleoecology, adaptations and the origins of bipedalism in Hominidae. In *Human Origins and Environmental Backgrounds* (ed. H. Ishida, R. H. Tuttle, M. Pickford, M. Ogihara and M. Nakatsukasa), pp. 175-198. Heidelberg: Springer.
Pickford, M., Senut, B., Gommery, D. and Treil, J. (2002). Bipedalism in *Orrorin tugenensis* revealed by its femora. *C. R. Palevol.* **1**, 191-203.
Polk, J. D. (2002). Adaptive and phylogenetic influences on musculoskeletal design in cercopithecine primates. *J. Exp. Biol.* **205**, 3399-3412.
Prost, J. H. (1980). Origin of bipedalism. *Am. J. Phys. Anthropol.* **52**, 175-198.
Richmond, B. G. and Jungers, W. L. (2008). *Orrorin tunegensis* femoral morphology and the evolution of hominin bipedalism. *Science* **319**, 1662-1665.
Sati, J. P. and Alfred, J. R. B. (2002). Locomotion and posture in Hoolock gibbon. *Ann. For.* **10**, 298-306.
Schmitt, D. and Larson, S. G. (1995). Heel contact as a function of substrate type and speed in primates. *Am. J. Phys. Anthropol.* **96**, 39-50.
Senut, B. (2003). Palaeontological approach to the evolution of hominid bipedalism: the evidence revisited. *Cour. Forsch.-Inst. Senkenberg* **243**, 125-134.
Senut, B. (2006). Arboreal origins of bipedalism. In *Human Origins and Environmental Backgrounds* (ed. H. Ishida, R. H. Tuttle, M. Pickford, N. Ogihara and M. Nakatsukasa), pp. 199-208. Heidelberg: Springer.
Simonsen, E. D., Dyhre-Poulsen, P., Voigt, M., Aagaard, P. and Falletin, N. (1997). Mechanisms contributing to different joint moments observed during human walking. *Scand. J. Med. Sci. Sports* **7**, 1-13.
Stern, J. T. (1975). Before bipedality. *Yearb. Phys. Anthropol.* **19**, 59-68.
Stern, J. T. and Susman, R. L. (1983). The locomotor anatomy of *Australopithecus afarensis*. *Am. J. Phys. Anthropol.* **60**, 279-317.
Thorpe, S. K. S., Holder, R. L. and Crompton, R. H. (2007). Origin of human bipedalism as an adaptation for locomotion on flexible branches. *Science* **316**, 1328-1331.
Tuttle, R. H. (1969). Knuckle-walking and the evolution of Hominoid hands. *Am. J. Phys. Anthropol.* **26**, 171-206.
Tuttle, R. H. (1981). Evolution of hominid bipedalism and prehensile capabilities. *Philos. Trans. R. Soc. Lond., B, Biol. Sci.* **292**, 89-94.
Vaughan, C. L. (1996). Are joint torques the Holy Grail of human gait analysis? *Hum. Mov. Sci.* **15**, 423-443.
Vereecke, E. E., D'Août, K., De Clercq, D., Van Elsacker, L. and Aerts, P. (2003). Dynamic plantar pressure distribution during terrestrial locomotion of bonobos (*Pan paniscus*). *Am. J. Phys. Anthropol.* **120**, 373-383.
Vereecke, E. E., D'Août, K., De Clercq, D., Van Elsacker, L. and Aerts, P. (2005a). Functional analysis of the gibbon foot during terrestrial bipedal walking: plantar pressure distributions and 3D ground reaction forces. *Am. J. Phys. Anthropol.* **128**, 659-669.
Vereecke, E. E., D'Août, K., Payne, R. and Aerts, P. (2005b). Functional analysis of the foot and ankle myology of gibbons and bonobos *J. Anat.* **206**, 453-476.
Vereecke, E. E., D'Août, K. and Aerts, P. (2006a). Speed modulation in hylobatid bipedalism: a kinematical analysis. *J. Hum. Evol.* **51**, 513-526.
Vereecke, E. E., D'Août, K. and Aerts, P. (2006b). The dynamics of hylobatid bipedalism: evidence for an energy-saving mechanism? *J. Exp. Biol.* **209**, 2829-2838.
Vereecke, E. E. and Van Sint Jan, S. (2008). The functional anatomy of the ape foot. In *Advances in Plantar Pressure Measurements in Clinical and Scientific Research* (ed. K. D'Août, K. Lescrenier and B. Van Gheluwe), pp. 89-106. Maastricht: Shaker Publishing BV.
Wells, R. P. (1981). The projection of ground reaction force as a predictor of internal joint moments. *Bull. Prosthet. Res.* **18**, 15-19.
Winter, D. A. (1990). *The Biomechanics and Motor Control of Human Movement*. 3rd edn. New York: Wiley.
Wolde Gabriel, G., Haile-Selassie, Y., Renne, P. R., Hart, W. K., Ambrose, S. H., Asfaw, B., Heiken, G. and Witte, T. (2001). Geology and palaeontology of the Late Miocene Middle Awash valley, Afar rift, Ethiopia. *Nature* **412**, 175-178.